IEEE Photonics Journal
An IEEE Photonics Society Publication

Open Access

High Conversion Efficiency Photonic Microwave Mixer With Image Rejection Capability

Volume 8, Number 4, August 2016

J. Zhang
E. H. W. Chan
X. Wang
X. Feng
B. Guan

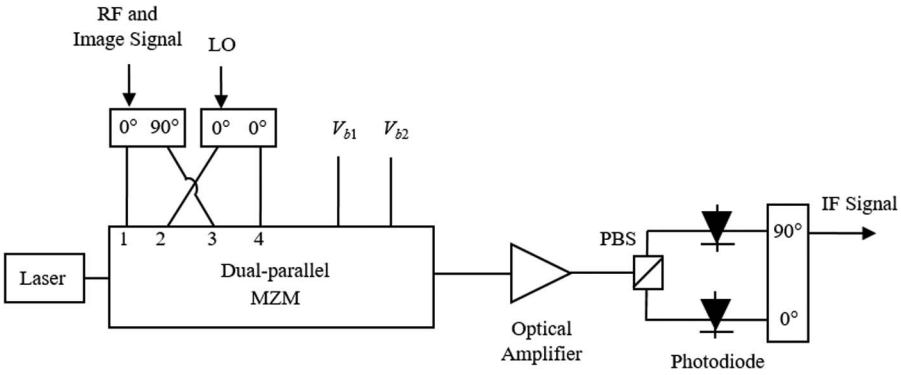

DOI: 10.1109/JPHOT.2016.2592327
1943-0655

High Conversion Efficiency Photonic Microwave Mixer With Image Rejection Capability

J. Zhang,[1] E. H. W. Chan,[2] X. Wang,[1] X. Feng,[1] and B. Guan[1]

[1]Guangdong Provincial Key Laboratory of Optical Fiber Sensing and Communications, Institute of Photonics Technology, Jinan University, Guangzhou 510632, China
[2]School of Engineering and Information Technology, Charles Darwin University, Darwin, NT 0909, Australia

DOI: 10.1109/JPHOT.2016.2592327

Manuscript received June 21, 2016; revised July 11, 2016; accepted July 13, 2016. Date of publication July 15, 2016; date of current version July 26, 2016. This work was supported in part by the National Natural Science Foundation of China under Grant 61475065 and Grant 61501205; by the Guangdong Natural Science Foundation under Grant 2014A030310419, Grant 2015A030313322, and Grant S2013030013302; and by the Fundamental Research Funds for the Central Universities under Grant 21615325. Corresponding author: X. Wang (e-mail: txudong.wang@email.jnu.edu.cn).

Abstract: A new photonic microwave image rejection mixer that can achieve high conversion efficiency and has a wide bandwidth is presented. It is based on an integrated dual-parallel Mach–Zehnder modulator (MZM) with a 90° polarization rotator on one branch of the modulator. The two modulators connected in parallel are biased at the minimum transmission point to generate two sets of orthogonally polarized radio frequency (RF) and local oscillator (LO) modulation sidebands with the optical carrier being suppressed. Suppressing the optical carrier enables high RF and LO modulation sidebands to be detected by a photodiode without saturation. The LO modulation index is also designed to obtain a high conversion efficiency mixing operation. Experimental results demonstrate frequency downconversion with an image rejection function and a high conversion efficiency of > -5 dB over a wide 3 to 20 GHz frequency range. A technique for compensating the effect of coupler amplitude and phase imbalance to obtain a high image rejection ratio is also experimentally demonstrated.

Index Terms: Fiber-optics communications, radio-frequency (RF) photonics, microwaves, analog optical signal processing.

1. Introduction

Signal processing in the optical domain provides the potential for very wide band operation, as the bandwidth of the modulated signal is very small compared with optical carrier frequency [1]. Photonics also provides improved electro-magnetic interference (EMI) and electro-magnetic compatibility (EMC) performance over traditional electronic systems, thereby providing more options for cable routing. The inherent opto-isolation of signals within a photonics-based processor provides tactical advantages through the reduction of re-radiated signals.

Microwave frequency mixing is one of the important signal processing functions for microwave and millimeter wave antenna applications such as radio-over-fiber [2] and defense receiver systems [3]. The function of a mixer is to up or down convert the frequency of a radio frequency (RF) signal into an intermediate frequency (IF) signal by mixing the RF signal with a

local oscillator (LO). Conventional electronic mixers have the problems of limited bandwidth, limited isolation, and EMI, which can be overcome by photonic microwave mixers. Various photonic microwave mixer structures have been reported [2]–[17]. Most of them are based on two optical modulators, where one is driven by an RF signal, and the other is driven by an LO arranged in different configurations. For example photonic microwave mixers can be implemented by connecting two MZMs in series [4], [5], two optical phase modulators in parallel [7] or series [8], an MZM and an electroabsorption modulator in series [9], two optical phase modulators inside a Sagnac loop interferometer [10] or two MZMs in parallel [11], [12]. Among them, mixers based on an integrated dual-parallel Mach–Zehnder modulator (MZM) is of interest as they have demonstrated the ability to obtain high conversion efficiency [11] and high spurious free dynamic range [12] mixing operation. Recently a dual-parallel MZM based mixer has been reported to realize an image rejection function [13]. The image signal, which is usually generated by a human source, is picked up by an antenna together with an RF signal. It has a frequency $f_{IM} = f_{LO} - f_{IF}$, which generates an unwanted signal at the IF signal frequency f_{IF} after it is mixed with an LO frequency f_{LO}. This unwanted signal causes false reception or distorts the wanted IF signal, which is generated by mixing the LO with an RF signal having a frequency $f_{RF} = f_{LO} + f_{IF}$. This problem can be solved by using an image rejection mixer. There are only few reports on photonics-based image rejection mixers [13]–[17]. They rely on using one or more optical filters to select one modulation sideband, which limits the mixer lower operating frequency [13], [14], or using multiple modulators, which increases the system loss [15]–[17]. Some of them also use electrical components such as amplifiers and filters [16], [17], which limit the system bandwidth. Until now there has been no report on a photonic microwave image rejection mixer that can achieve high conversion efficiency over a wide frequency range.

This paper presents a photonic microwave mixer based on an integrated dual-parallel MZM that not only can suppress the effect of an image signal but also has high conversion efficiency and a wide bandwidth. The ability of rejecting an image signal and realizing high conversion efficiency mixing operation are analyzed. Experiments are preformed to demonstrate the ideas. A technique of introducing attenuation and time delay in the mixer structure, which was used in the balanced detection structure for laser intensity noise suppression [18], to compensate for the effect of amplitude and phase imbalance of the couplers used in the system is also presented and experimentally verified.

2. Topology and Operation Principle

The topology of the high conversion efficiency photonic microwave image rejection mixer is shown in Fig. 1(a). A laser source generating a continuous wave light with linear polarization aligned to the slow axis is launched into an integrated dual-parallel MZM having a structure as shown in Fig. 1(b). The modulator consists of two dual-drive MZMs connected in parallel. Each dual-drive MZM has a Mach–Zehnder structure with a phase modulator (PM) in each branch. It has two RF ports, and a DC port for inputting a bias voltage to control the phase difference between the two branches. The output of the lower MZM is connected to a 90° polarization rotator. Hence the polarization state of the light after the 90° polarization rotator is orthogonal to that at the output of the upper MZM. The two orthogonally polarized signals are combined by a polarization beam combiner (PBC). Fig. 1 shows the upper and lower dual-drive MZMs inside the dual-parallel MZM are driven by a 90° phase different RF and image signal and an LO. The modulators are biased at the minimum transmission point to suppress the optical carrier, which is normally several orders of magnitude higher than the sidebands and has no contribution to the frequency conversion process, leaving two sets of orthogonally polarized RF and image signal modulation sidebands and LO modulation sidebands at the dual-parallel MZM output. An optical amplifier can be used to amplify the sidebands. The orthogonally polarized modulation sidebands are split by a polarization beam splitter (PBS) so that the sidebands aligned to the slow and fast axis are detected by the top and bottom photodiode, respectively. Two IF signals

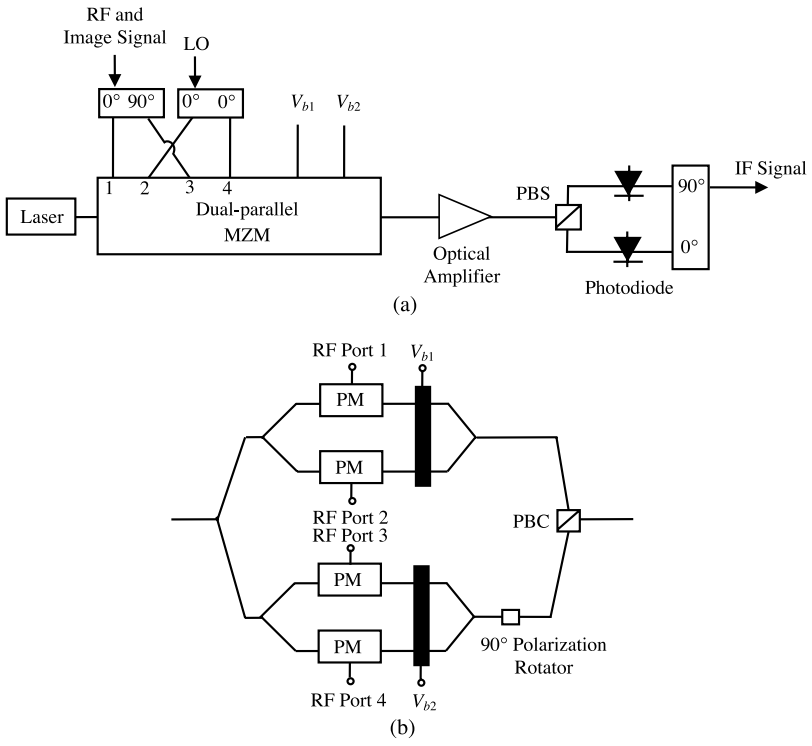

Fig. 1. (a) Structure of the dual-parallel MZM-based photonic microwave image rejection mixer and (b) the inner structure of an integrated dual-parallel MZM.

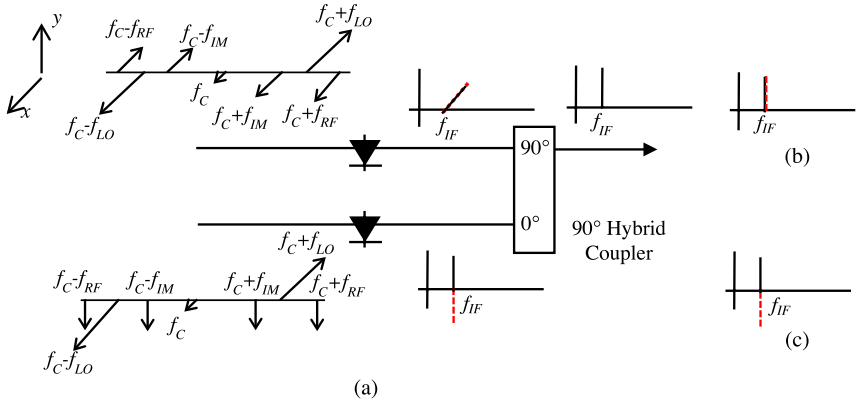

Fig. 2. (a) RF and image signal and LO modulation sidebands incident on the photodiodes and the mixer output spectrum showing that the unwanted signal at the IF signal frequency f_{IF} is cancelled after the 90° hybrid coupler. The IF signal (——) and the unwanted signal (- - -) after the photodiode is generated by an RF and image signal beats with an LO, respectively. The IF signal and the unwanted signal from (b) the upper and (c) the lower branch of the dual-parallel MZM after the 90° hybrid coupler.

having different phases are produced at the two photodiode outputs. A 90° hybrid coupler is used to combine the photodiode outputs and to suppress the unwanted signal at the IF signal frequency, which is generated by an image signal mixed with an LO.

Fig. 2 shows the suppressed carrier at the frequency f_c together with the modulation sidebands after the PBS into the photodiodes. Note that the x and y axis in the figure indicate the in-phase and quadrature component respectively. The RF and image signal and LO modulation sidebands beat at the photodiode, generating an IF signal at the frequency f_{IF}. Fig. 2 illustrates

the case where the mixer is used for downconversion in which the frequency of the RF signal, image signal, and LO are in the GHz to tens of GHz range, and the downconverted IF signal frequency is in the hundreds of megahertz range. The RF signal, image signal, LO, and IF signal have the following frequency relationships: $f_{RF} = f_{LO} + f_{IF}$, $f_{IM} = f_{LO} - f_{IF}$ and $f_{RF} > f_{LO} > f_{IM} \gg f_{IF}$. It can be seen from Fig. 2 that the IF signal generated by an RF signal beats with an LO at output of the top photodiode has the same phase as that generated by an image signal beats with the LO. On the other hand, the IF signals at the output of the bottom photodiode have an opposite phase. The 90° hybrid coupler after the photodiodes introduces a 90° phase shift to the IF signals after the top photodiode and combines with the IF signals at the bottom photodiode output. As a result, the IF signals generated by the RF signal beats with an LO at the two photodiode outputs are in phase, whereas the IF signals generated by the image signal beats with the LO at the two photodiode outputs are out of phase and are cancelled after the 90° hybrid coupler. This shows the mixer has the ability to reject the effect of an image signal to the mixer output.

Although both the mixer shown in Fig. 1 and the mixer presented in [13] are implemented by using a dual-parallel MZM and have the image rejection function, their operation principles are different. In [13], the modulator bias voltages are designed to obtain a 90° phase shift, whereas the modulators in the mixer shown in Fig. 1 are biased at the minimum transmission point to suppress the optical carrier. In [13], an optical filter with sharp edge roll-off is required to select only one modulation sideband at the dual-parallel MZM output. This limits the system lower operating frequency to around 10 GHz. As such the mixer cannot be used for 1–18 GHz and 4–40 GHz electronic warfare systems [3], [7]. Using an optical filter in the setup not only introduces an additional loss in the system, which reduces the sideband amplitude by as much as 12 dB [13], but also filters out one sideband, which is clearly not efficient compared to using both upper and lower modulation sidebands for frequency conversion in the mixer shown in Fig. 1, degrading the mixer conversion efficiency and noise figure performance. A sharp edge roll-off optical filter is not required in the image rejection mixer shown in Fig. 1. In this case, the mixer also has the advantage that its output is not sensitive to changes in the laser source wavelength.

3. Analysis and Simulation

Referring to Fig. 1, the electric field at the output of the upper MZM driven by an RF signal, an image signal and an LO having an angular frequency ω_{RF}, ω_{IM} and ω_{LO}, respectively, can be expressed as

$$E_{top}(t) = \frac{E_{in}\sqrt{t_{ff}}}{4}\left[\begin{array}{c}\cos(\omega_c t + \beta_{RF}\sin\omega_{RF} t + \beta_{IM}\sin\omega_{IM} t) \\ + \cos(\omega_c t + \beta_{LO}\sin\omega_{LO} t + \pi)\end{array}\right] \quad (1)$$

where E_{in} is the electric field amplitude of the light at the dual-parallel MZM input; t_{ff} is the MZM insertion loss; ω_c is the angular frequency of the light into the MZM; $\beta_{RF} = \pi V_{RF}/V_\pi$, $\beta_{IM} = \pi V_{IM}/V_\pi$ and $\beta_{LO} = \pi V_{LO}/V_\pi$ are the modulation index of the input RF signal, image signal, and LO, respectively; and V_π is the modulator switching voltage. The electric field at the output of the lower MZM driven by the same LO and the same RF and image signal but with a 90° phase shift to that applied to the upper MZM can be expressed as

$$E_{bottom}(t) = \frac{E_{in}\sqrt{t_{ff}}}{4}\left[\begin{array}{c}\cos(\omega_c t + \beta_{RF}\sin(\omega_{RF} t + 90°) + \beta_{IM}\sin(\omega_{IM} t + 90°)) \\ + \cos(\omega_c t + \beta_{LO}\sin\omega_{LO} t + \pi)\end{array}\right]. \quad (2)$$

The 90° polarization rotator after the lower MZM rotates the light polarization state by 90° so that the polarization of the light at the output of the lower branch of the integrated dual-parallel MZM is aligned to the fast axis. Therefore, the electric field after the dual-parallel MZM is given by

$$E_{DPMZM}(t) = \hat{x}E_{top}(t) + \hat{y}E_{bottom}(t) \quad (3)$$

where $\hat{x}$ and $\hat{y}$ represent the two orthogonal polarization states. Under small signal conditions, the electric field after the dual-parallel MZM can be written as

$$E_{\mathrm{DPMZM}}(t) = \frac{E_{\mathrm{in}}}{4}\sqrt{t_{\mathrm{ff}}}\left\{\begin{array}{l}\hat{x}\left[\begin{array}{c}(1-J_0(\beta_{\mathrm{LO}}))\cos\omega_c t\\ -\frac{\beta_{\mathrm{RF}}}{2}(\cos(\omega_c-\omega_{\mathrm{RF}})t-\cos(\omega_c+\omega_{\mathrm{RF}})t)\\ -\frac{\beta_{\mathrm{IM}}}{2}(\cos(\omega_c-\omega_{\mathrm{IM}})t-\cos(\omega_c+\omega_{\mathrm{IM}})t)\\ +J_1(\beta_{\mathrm{LO}})(\cos(\omega_c-\omega_{\mathrm{LO}})t-\cos(\omega_c+\omega_{\mathrm{LO}})t)\end{array}\right]\\ +\hat{y}\left[\begin{array}{c}(1-J_0(\beta_{\mathrm{LO}}))\cos\omega_c t\\ -\frac{\beta_{\mathrm{RF}}}{2}(\sin(\omega_c-\omega_{\mathrm{RF}})t+\sin(\omega_c+\omega_{\mathrm{RF}})t)\\ -\frac{\beta_{\mathrm{IM}}}{2}(\sin(\omega_c-\omega_{\mathrm{IM}})t+\sin(\omega_c+\omega_{\mathrm{IM}})t)\\ +J_1(\beta_{\mathrm{LO}})(\cos(\omega_c-\omega_{\mathrm{LO}})t-\cos(\omega_c+\omega_{\mathrm{LO}})t)\end{array}\right]\end{array}\right\} \tag{4}$$

where $J_m(x)$ is the Bessel function of the mth order of the first kind. Note from (4) that the phase of the RF and image signal modulation sidebands are different for the two orthogonally polarized signals. The PBS splits the two orthogonally polarized signals. The optical signal with $\hat{x}$ and $\hat{y}$ polarization state are detected by the top and bottom photodiode respectively. Since the optical power is the electric field square, i.e., $P = |E|^2$, and the photocurrent is the product of the optical power and photodiode responsivity $\Re$, the photocurrents at the IF signal angular frequency, i.e., $\omega_{\mathrm{IF}} = \omega_{\mathrm{RF}} - \omega_{\mathrm{LO}} = \omega_{\mathrm{LO}} - \omega_{\mathrm{IM}}$, generated at the output of the two photodiodes can be obtained from (4) and are written as

$$I_{\mathrm{IF,top}} = \frac{1}{16}\Re P_{\mathrm{in}} G_{\mathrm{OA}} t_{\mathrm{ff}} J_1(\beta_{\mathrm{LO}})[-\beta_{\mathrm{RF}}\cos(\omega_{\mathrm{RF}}-\omega_{\mathrm{LO}})t - \beta_{\mathrm{IM}}\cos(\omega_{\mathrm{LO}}-\omega_{\mathrm{IM}})t] \tag{5}$$

$$I_{\mathrm{IF,bottom}} = \frac{1}{16}\Re P_{\mathrm{in}} G_{\mathrm{OA}} t_{\mathrm{ff}} J_1(\beta_{\mathrm{LO}})[\beta_{\mathrm{RF}}\sin(\omega_{\mathrm{RF}}-\omega_{\mathrm{LO}})t - \beta_{\mathrm{IM}}\sin(\omega_{\mathrm{LO}}-\omega_{\mathrm{IM}})t] \tag{6}$$

where P_{in} is the optical power into the dual-parallel MZM, and G_{OA} is the gain of the optical amplifier after the dual-parallel MZM. The 90° hybrid coupler connected to the photodiode output shifts the phase of the IF signal at the top photodiode output by 90°. Therefore the mixer output at the IF signal frequency can be written as

$$I_{\mathrm{IF}} = \frac{1}{8}\Re P_{\mathrm{in}} G_{\mathrm{OA}} t_{\mathrm{ff}} \beta_{\mathrm{RF}} J_1(\beta_{\mathrm{LO}})\sqrt{L_{\mathrm{out}}}\sin(\omega_{\mathrm{RF}}-\omega_{\mathrm{LO}})t \tag{7}$$

where L_{out} is the insertion loss of the 90° hybrid coupler at the mixer output. Equation (7) shows the IF signal generated from the image signal is cancelled but the IF signal generated from the RF signal remains demonstrating the image rejection mixing operation. The mixer conversion efficiency, which is defined as the ratio of the output IF signal power to the input RF signal power [6], can be obtained from (7) and is given by

$$G = \frac{1}{64}\Re^2 P_{\mathrm{in}}^2 G_{\mathrm{OA}}^2 t_{\mathrm{ff}}^2 \left(\frac{\pi}{V_\pi}\right)^2 J_1^2(\beta_{\mathrm{LO}}) L_{\mathrm{in}} L_{\mathrm{out}} R_{\mathrm{in}} R_{\mathrm{out}} \tag{8}$$

where L_{in} is the insertion loss of the 90° hybrid coupler at the mixer input, R_{in} is the modulator input resistance and R_{out} is the photodiode load resistance. Equation (8) shows the image rejection mixer conversion efficiency can be improved by increasing the optical power into the photodiode by using either high laser source power or high optical amplifier gain. However, in practice photodiodes have limited optical power handling ability, e.g., commercial photodiodes can handle 18 dBm optical power [19]. Therefore the laser source power and the optical amplifier gain need to be designed to obtained high conversion efficiency without saturating the photodiodes. The average optical power into the photodiode for the image rejection mixer shown in Fig. 1 is given by

$$P_{\mathrm{avg}} = \frac{1}{16} P_{\mathrm{in}} G_{\mathrm{OA}} t_{\mathrm{ff}} \left[\frac{(1-J_0(\beta_{\mathrm{LO}}))^2}{2} + \frac{\beta_{\mathrm{RF}}^2}{4} + \frac{\beta_{\mathrm{IM}}^2}{4} + J_1^2(\beta_{\mathrm{LO}})\right]. \tag{9}$$

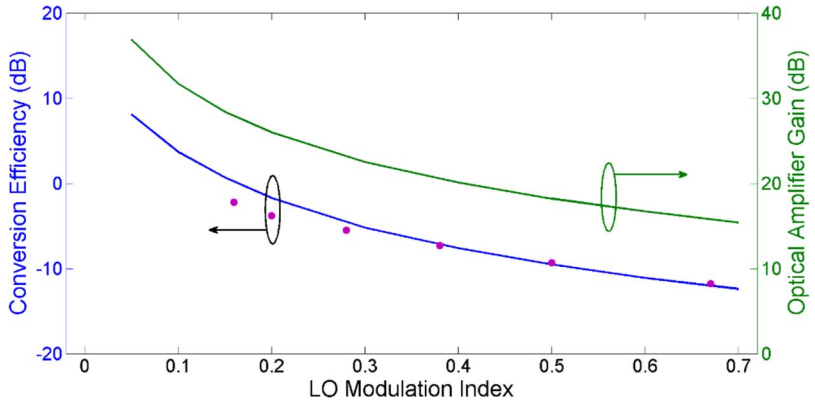

Fig. 3. Simulated (—) and measured (●) mixer conversion efficiency versus LO modulation index. The optical amplifier gain required for different LO modulation indexes to fix the average output optical power to be 10 dBm is also shown. The value of the parameters used in the simulation are $V_\pi = 8.3$ V, $\Re = 0.7$ A/W, and $L_{\text{in}} = L_{out} = 5$ dB.

Since the two modulators inside the integrated dual-parallel MZM structure are biased at the minimum transmission point, the optical carrier is suppressed and hence the average optical power into the photodiode is mainly determined by the power of the LO modulation sidebands. Note that (8) and (9) show both the mixer conversion efficiency and the average optical power into the photodiode are proportional to the square of the first order Bessel function of the LO modulation index $J_1(\beta_{\text{LO}})^2$. However, it can be seen from the equations that the mixer conversion efficiency is proportional to the optical amplifier gain square G_{OA}^2 whereas the average optical power into the photodiode is proportional to G_{OA}. Therefore one can reduce the LO modulation index and increase the optical amplifier gain to maintain the same amount of optical power into the photodiode, i.e., to avoid saturating the photodiode, and at the same time increase the mixer conversion efficiency. Note that for simplicity the above analysis assumes the RF signal, the image signal and the LO are a single frequency sinusoidal wave as was used in the reported photonic microwave image rejection mixer analysis. The dual-parallel MZM based photonic microwave image rejection mixer is suitable for up or down converting a practical RF signal, which has a band of frequency and has arbitrary amplitude and phase. This has been verified using VPITransmissionMarker photonic simulation software by simultaneously applying multiple RF signals with different amplitude, frequency and phase into the dual-parallel MZM based image rejection mixer.

Fig. 3 shows the simulation results of the image rejection mixer conversion efficiency as a function of the LO modulation index where the optical amplifier gain is adjusted so that the average optical power into the photodiode is fixed at 10 dBm. This shows high conversion efficiency can be obtained using small LO modulation index and high optical amplifier gain. Positive conversion efficiency, i.e., conversion gain, can be obtained when $\beta_{\text{LO}} < 0.17$. The conversion efficiency of the dual-parallel MZM based image rejection mixer is similar to that of the mixers, which were designed to obtain high conversion efficiency performance [8], [10], [11], and is largely improved compared to the conventional cascaded-modulator based photonic microwave mixers [4], [5]. In additional to high conversion efficiency, the image rejection mixer also exhibits high isolation between the RF and LO ports. Biasing the modulators in the dual-parallel MZM structure at the minimum transmission point to suppress the optical carrier not only can improve the mixer conversion efficiency but also suppress the RF and LO frequency components at the mixer output. This cannot be obtained using the conventional cascaded-modulator based photonic microwave mixers [4], [5], which have the problem of generating unwanted spurious terms at the mixer output due to the present of the strong LO frequency component [6]. It should be pointed out that although commercial image rejection mixers can operate at high frequencies, they have a limited bandwidth, which limits their use in applications such as defense that

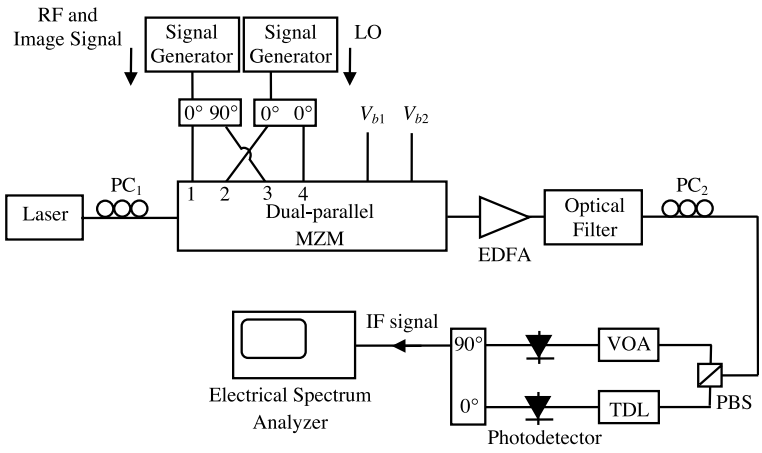

Fig. 4. Experimental setup of the photonic microwave image rejection mixer.

requires wide bandwidth. Currently, commercial image rejection mixers have the advantage in terms of cost and size. However, silicon photonic technology, which enables integrating both active and passive photonic devices in a silicon chip [20], can significantly reduce the cost and size of the dual-parallel MZM based photonic microwave image rejection mixer. It was stated in [21] that analog photonic technologies into the W band (75–110 GHz) are now commercially available. The dual-parallel MZM based photonic microwave image rejection mixer operating frequency is limited by the 90° hybrid couplers. Nevertheless commercial 90° hybrid couplers have a 4–67 GHz bandwidth [22] indicating the mixer can be operated in the V band (57–66 GHz).

4. Experimental Results

Experiments were set up as shown in Fig. 4 to verify the concept of the photonic microwave image rejection mixer. The optical source used in the experiment had a 1550 nm wavelength and 100 kHz linewidth. The continuous wave light from the laser source, after passing through a polarization controller (PC_1), was launched into an integrated dual-parallel MZM (Fujitsu FTM7980). Both the upper and lower MZMs inside the integrated modulator structure were biased at the minimum transmission point. Over 40 dB carrier suppression was measured at the modulator output. PC_1 was used to align the light polarization state into the integrated dual-parallel MZM to maximize the modulation efficiency. Two 20 GHz microwave signal generators (Agilent 83752A, Anritsu MG3692B) were used to provide an RF or image signal and an LO, and were connected to the input of a 2–26.5 GHz 90° hybrid coupler (Marki Microwave QH0226) and a 1–40 GHz Wilkinson power divider (Marki Microwave PD0140) respectively. The outputs of the 90° hybrid coupler were connected to Port 1 and 3 of the modulator. The outputs of the Wilkinson power divider were connected to Port 2 and 4 of the modulator. The orthogonally polarized modulation sidebands at the modulator output were amplified by an erbium-doped fiber amplifier (EDFA), which was followed by an optical filter to filter out the amplified spontaneous emission noise from the amplifier. The optical filter had 1 nm bandwidth, 1550 nm center wavelength and 1 dB insertion loss. Since the EDFA and the optical filter were not polarization maintaining components, PC_2 was used to align the polarization states of the orthogonally polarized modulation sidebands into a PBS whose outputs were connected to two 50 GHz bandwidth photodetector (U2t XPDV2120R) to generate two IF signals. It should be noted that PC_1 and PC_2 can be avoided by using polarization maintaining components between the laser and the PBS. A variable optical attenuator (VOA) and a tunable delay line (TDL) were connected between the PBS and the photodetectors to match the amplitude of the IF signals at the photodetector outputs and to control the path length difference between the PBS and the photodetector. The two IF signals were combined by a 0.5–9 GHz 90° hybrid coupler (Gwave GHC-90-005090). The output of the coupler was viewed on an electrical spectrum analyzer (Anritsu MS2692A).

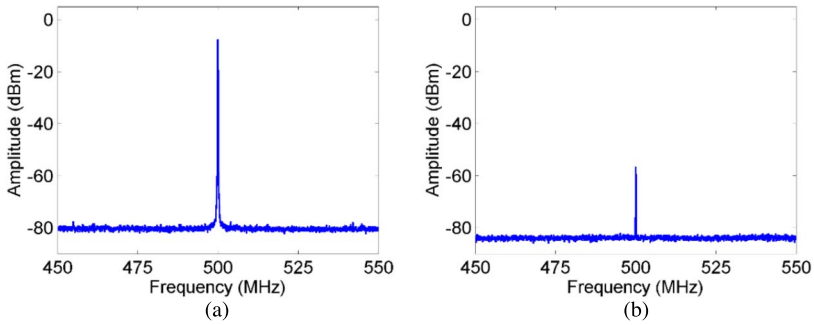

Fig. 5. Measured mixer output IF signal generated by (a) a 20-GHz RF signal and (b) a 19-GHz image signal mixed with a 19.5-GHz LO.

Due to the frequency limitation of the signal generators used in the experiment, the RF signal frequency, the LO frequency and the image signal frequency were designed to be 20 GHz, 19.5 GHz, and 19 GHz, respectively. Therefore the mixer output IF signal frequency was 500 MHz. The input RF and image signal power measured on the electrical spectrum analyzer were -2.5 dBm. The VOA and TDL were adjusted to maximize the mixer image rejection ratio, which is defined as the ratio of the wanted and unwanted IF signal power. The mixer conversion efficiency was measured for different LO powers while the optical powers into the two photodetectors were fixed at 10 dBm by adjusting the EDFA gain. The measured conversion efficiencies for different LO modulation indexes are shown in Fig. 3. This verifies high conversion efficiency can be obtained using a small LO modulation index. The mixer conversion efficiency is -2.2 dB for 0.16 LO modulation index, which is around 5 dB above the conversion efficiency of the current state-of-art commercial image rejection mixers [23], [24]. With an LO modulation index of 0.16, the mixer output IF signals generated by the RF and image signal beat with the LO were measured on the electrical spectrum analyzer and are shown in Fig. 5(a) and (b) respectively. It can be seen from the figure that the wanted and unwanted IF signal power are -4.6 dBm and -56.5 dBm, respectively. This corresponds to a 51.9 dB image rejection ratio. It should be pointed out again that the unwanted frequency component generated by the image signal mixed with the LO has the same frequency as the IF signal. Therefore the RF signal and the image signal were applied separately to the modulator in order to measure the amplitude of the IF signal and the unwanted frequency component at 500 MHz.

In order to investigate the performance of the photonic microwave image rejection mixer over a wide frequency range, the frequency of the RF signal, the LO and the image signal were tuned from 3–20 GHz, 2.5–19.5 GHz, and 2–19 GHz respectively with an IF signal frequency fixed at 500 MHz. Fig. 6 shows the mixer conversion efficiency is > -5 dB over the 3 to 20 GHz input RF signal frequency range. This is 15 dB above the conversion efficiency of the recently reported image rejection mixer [13]. Note from Fig. 6 that the mixer conversion efficiency has < 3 dB variation over the 3 to 20 GHz frequency range. This variation is due to the frequency characteristic of the modulator, hybrid couplers, photodiodes, and cables used in the experiment. Using components with a flatter frequency response performance can reduce the mixer conversion efficiency variation.

The mixer image rejection ratio was also measured for different RF signal frequencies while the IF signal frequency was fixed at 500 MHz. Fig. 7 (▼) shows the image rejection ratio changes with the RF signal frequency and it reduces to 28.4 dB for 3 GHz RF signal frequency. The frequency-dependent image rejection ratio measured in the experiment is due to the frequency dependent characteristic of the couplers used in the setup. In practice, couplers have amplitude and phase imbalance, which degrades the image rejection ratio [15]. Since the amplitude and phase imbalance of a coupler are different at difference frequencies, the mixer image rejection ratio is frequency dependent. The amplitude imbalance in the couplers can be compensated by using a VOA to control the optical power into the photodetector. The attenuation of

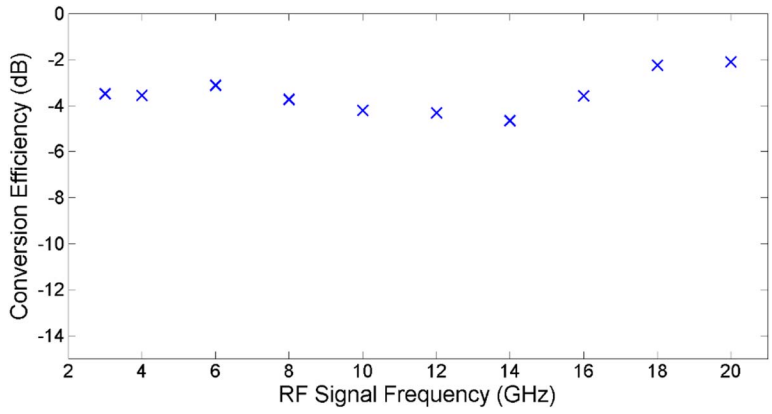

Fig. 6. Measured mixer conversion efficiency for different input RF signal frequencies.

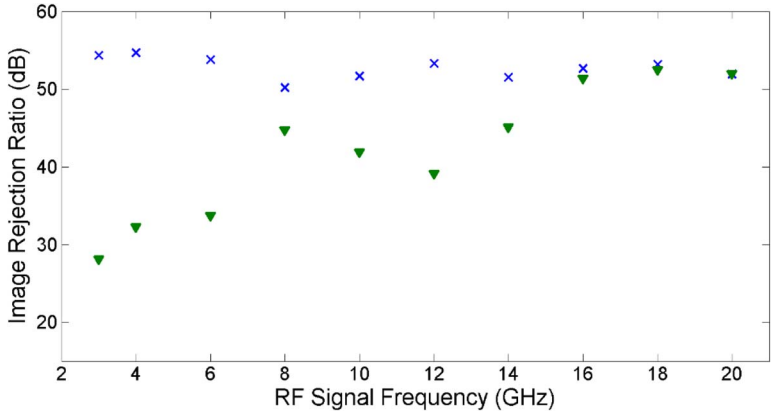

Fig. 7. Measured mixer image rejection ratio for different input RF signal frequencies with (×) and without (▼) adjusting the VOA and the TDL.

the VOA needs to be adjusted as the input RF signal frequency changes to compensate for the effect of the frequency dependent amplitude imbalance in the couplers. Similarly the phase imbalance in the couplers can be compensated by using a TDL to introduce a frequency dependent phase shift. Therefore in practice one can use a programmable VOA and a programmable TDL to maintain high image rejection ratio as the input RF signal frequency changes. This has been experimentally verified with the results shown in Fig. 7 (×). It can be seen that $>$ 50 dB image rejection ratio was maintained as the RF signal frequency changes over the 3–20 GHz frequency range. Note that the typical bandwidth of an IF signal is few 100 MHz [5], [8]. While fixing the VOA and TDL setting at the optimum value for 18 GHz RF signal frequency, the mixer image rejection ratio was measured over a range of frequency around 18 GHz. The experimental result in Fig. 8 shows over 40 dB image rejection ratio can be maintained in a 500 MHz frequency band. The same measurement was conducted at other RF signal frequencies and the experimental results show $>$ 40 dB image rejection ratio over a few 100 MHz frequency band can be obtained. This is more than 10 dB improvement compared to commercial image rejection mixers, which have a typical image rejection ratio of 25 to 30 dB. It should be pointed out that though the image rejection mixer presented in [13] does not require a 90° hybrid coupler, broadband power splitters are required to split an RF or image signal and an LO before entering the modulators. Broadband power splitters also have the problem of amplitude and phase imbalance, which affects the mixer image rejection ratio. This problem was not discussed in the paper.

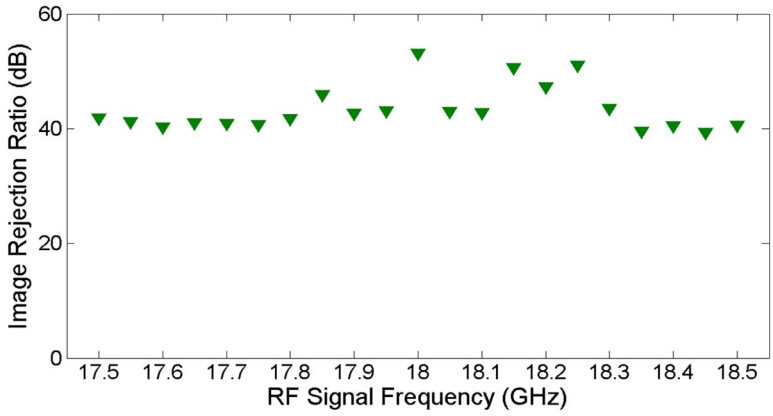

Fig. 8. Measured mixer image rejection ratio within 1-GHz frequency band of an input RF signal at 18 GHz.

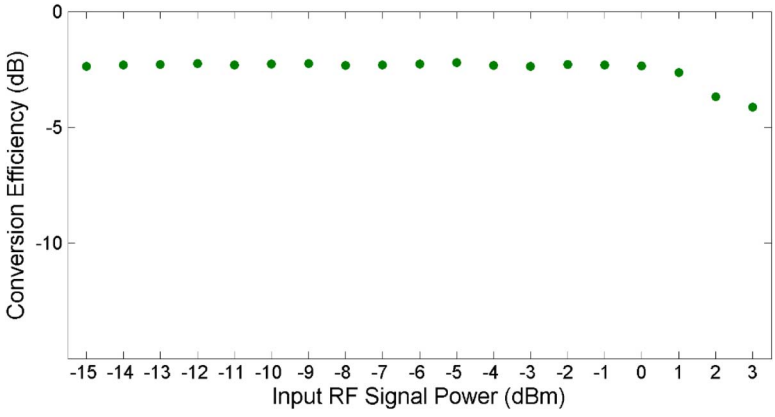

Fig. 9. Measured mixer conversion efficiency for different input RF signal powers.

Finally, the mixer conversion efficiency for different input RF signal powers was measured. This was done by changing the RF signal power from the signal generator (Agilent 83752A) in the range of -15 dBm to 3 dBm while fixing the RF signal and LO frequency to be 20 GHz and 19.5 GHz, respectively. The measurement shown in Fig. 9 indicates that the mixer conversion efficiency remains unchanged for the input RF signal power of < 0 dBm. This shows the mixer has a high conversion efficiency performance and can be operated over a wide RF power range. Note that the mixer conversion efficiency analysis assumes the RF signal is a small signal and hence (8) shows the mixer conversion efficiency is independent to the input RF signal power. However, as the input RF signal power increases, the condition of small RF signal is no longer valid. Under this condition the modulator nonlinearity needs to be taken into account and hence the output IF signal power is no longer increased linearly with the input RF signal power. Therefore the mixer conversion efficiency reduces as the RF signal power > 0 dBm, as shown in Fig. 9.

5. Conclusion

A novel photonic microwave signal processor for frequency down conversion has been presented. It has the ability of rejecting the effect of an image signal at the mixer output and simultaneously obtaining high conversion efficiency performance. It can be operated over a wide frequency range. The mixer conversion efficiency has been analyzed. The system parameters such as the LO modulation index and the optical amplifier gain have been designed to maximize

the conversion efficiency. Experimental results demonstrated the image rejection mixer has > -5 dB conversion efficiency over the 3–20 GHz RF signal frequency range. To the best of our knowledge, this is the highest reported conversion efficiency in a broadband image rejection mixer. A technique to compensate for the effect of the coupler amplitude and phase imbalance on the mixer image rejection ratio has also been presented and demonstrated experimentally.

Acknowledgment

The authors gratefully acknowledge B. Chen for her assistance with the experiments.

References

[1] R. A. Minasian, E. H. W. Chan, and X. Yi, "Microwave photonic signal processing," *Opt. Exp.*, vol. 21, no. 19, pp. 22918–22936, Sep. 2013.
[2] C. S. Park, C. G. Lee, and C. S. Park, "Photonic frequency upconversion by SBS-based frequency tripling," *J. Lightw. Technol.*, vol. 25, no. 7, pp. 1711–1718, Jul. 2007.
[3] A. C. Lindsay, G. A. Knight, and S. T. Winnall, "Photonic mixers for wide bandwidth RF receiver applications," *IEEE Trans. Microw. Theory Tech.*, 43, no. 9, pp. 2311–2317, Sep. 1995.
[4] G. K. Gopalakrishnan, W. K. Burns, and C. H. Bulmer, "Microwave-optical mixing in LiNbO3 modulators," *IEEE Trans. Microw. Theory Tech.*, vol. 41, no. 12, pp. 2383–2391, Dec. 1993.
[5] G. K. Gopalakrishnan, R. P. Moeller, M. M. Howerton, W. K. Burns, K. J. Williams, and R. D. Esman, "A low-loss downconverting analog fiber-optic link," *IEEE Trans. Microw. Theory Tech.*, vol. 43, no. 9, pp. 2318–2323, Sep. 1995.
[6] Y. Shi, W. Wang, and J. H. Bechtel, "High-isolation photonic microwave mixer/link for wideband signal processing and transmission," *J. Lightw. Technol.*, vol. 21, no. 5, pp. 1224–1232, May 2003.
[7] S. R. O'Connor, M. C. Gross, M. L. Dennis, and T. R. Clark, Jr., "Experimental demonstration of RF photonic down-conversion from 4–40 GHz," in *Proc. IEEE Int. Top. Meet. Microw. Photon.*, Oct. 2009, pp. 1–3.
[8] B. M. Haas and T. E. Murphy, "A carrier-suppressed phase-modulated fiber optic link with IF downconversion of 30 GHz 64-QAM signals," *Proc. IEEE Int. Top. Meet. Microw. Photon.*, Oct. 2009, pp. 1–4.
[9] R. Zhu, B. Hraimel, and X. Zhang, "Analysis of simultaneous photonic frequency downconversion and optical sub-carrier modulation in an electroabsorption modulator," *J. Lightw. Technol.*, vol. 30, no. 3, pp. 344–354, Feb. 2012.
[10] E. H. W. Chan and R. A. Minasian, "Microwave photonic downconversion using phase modulators in a Sagnac loop interferometer," *IEEE J. Sel. Topics Quant. Electron.*, vol. 19, no. 6, Nov. 2013, Art. no. 3500208.
[11] E. H. W. Chan and R. A. Minasian, "Microwave photonic downconverter with high conversion efficiency," *J. Lightw. Technol.*, vol. 30, no. 23, pp. 3580–3585, Dec. 2012.
[12] A. Altaqui, E. H. W. Chan, and R. A. Minasian, "Microwave photonic mixer with high spurious-free dynamic range," *Appl. Opt.*, vol. 53, no. 17, pp. 3687–3695, Jun. 2014.
[13] Z. Tang and S. Pan, "Image-reject mixer with large suppression of mixing spurs based on a photonic microwave phase shifter," *J. Lightw. Technol.*, to be published.
[14] S. Pan and Z. Tang, "A highly reconfigurable photonic microwave frequency mixer," in *Proc. SPIE Newsroom*, pp. 1–3, Feb. 2015, doi: 10.1117/2.1201501.005736.
[15] L. Chao, C. Wenyue, and J. F. Shiang, "Photonic mixers and image-rejection mixers for optical SCM systems," *IEEE Trans. Microw. Theory Tech.*, vol. 45, no. 8, pp. 1478–1480, Aug. 1997.
[16] S. J. Strutz, P. Biernacki, L. Nichols, and K. J. Williams, "Demonstration of a wide-band image rejection microwave downconverter," *IEEE Photon. Technol. Lett.*, vol. 12, no. 6, pp. 687–689, Jun. 2000.
[17] S. J. Strutz and K. J. Williams, "A 0.8–8.8-GHz image rejection microwave photonic downconverter," *IEEE Photon. Technol. Lett.*, vol. 12, no. 10, pp. 1376–1378, Oct. 2000.
[18] M. S. Islam *et al.,* "Distributed balanced photodetectors for broad-band noise suppression," *IEEE Trans. Microw. Theory Tech.*, vol. 47, no. 7, pp. 1282–1287, Jul. 1999.
[19] Finisar, *50 GHz High-Power Photodetector HPDV2120R Datasheet.* [Online]. Available: http://www.finisar.com.
[20] R. Won, "Microwave photonics shines," *Nature Photon.*, vol. 5, p. 736, Dec. 2011.
[21] V. J. Urick, C. S. Sunderman, J. F. Diehl, and N. D. Peterson, "W-band technology and techniques for analog millimeter-wave photonics," Naval Res. Lab., Washington, DC, USA, NRL/MR/5651-15-9624, Aug. 2015.
[22] ET Industries, "*Stripline 90 Degree Hybrid Coupler Q-467-90 Datasheet.*" [Online]. Available from: http://www.etiworld.com.
[23] Marki Microwave, *IQ Mixer Datasheet.* [Online]. Available from: http://www.markimicrowave.com.
[24] Millitech, *I/Q Mixer Datasheet.* [Online]. Available: http://www.millitech.com.